Nano-optofluidic detection of single viruses and nanoparticles

Anirban Mitra,[†] Bradley Deutsch,[‡] Filipp Ignatovich,[‡] Carrie Dykes,[¶] and Lukas Novotny[*,‡,†]

Department of Physics and Astronomy, Institute of Optics, and Department of Medicine, University of Rochester, Rochester NY 14627.

E-mail: novotny@optics.rochester.edu

Supporting Information Available

Theory

Let us consider the field $\mathbf{E}_\mathrm{s}$ generated by a particle with dipole $\mathbf{p}$ located at $\mathbf{r} = (x,y,z)$ and oriented transverse to the optical axis z (c.f. Fig. Figure 1). The radiated field is collected with an objective lens characterized by the focal length f and the numerical aperture $NA = n\sin\theta_\mathrm{max}$, with n being the index of refraction and θ_max the maximum collection angle measured from the optical axis. The dipole's farfield can be represented as[1]

$$\mathbf{E}_\mathrm{s}(\mathbf{r}_\infty) \;=\; \frac{k^2}{\varepsilon_o n^2}\,\frac{\exp(ikR - i\omega t)}{4\pi R}\,\left[\mathbf{I} - \mathbf{RR}/R^2\right]\mathbf{p}\,. \tag{1}$$

[†]Department of Physics and Astronomy, University of Rochester, Rochester NY 14627
[‡]Institute of Optics, University of Rochester, Rochester NY 14627
[¶]Department of Medicine, Infectious Diseases Division, University of Rochester, Rochester NY 14627

where $k = n\omega/c$ and $\mathbf{R} = \mathbf{r}_\infty - \mathbf{r}$ is the vector from dipole to the field point $\mathbf{r}_\infty$. For $\mathbf{r}_\infty$ located on the reference sphere of the lens and for small deviations of the dipole from the focus $\mathbf{r} = 0$ we expand R as

$$R \;=\; f - \frac{1}{f}\left[x x_\infty + y y_\infty + z z_\infty\right] + .. \tag{2}$$

Retaining only terms up to first-order in the phase and terms up to zeroth-order in the amplitude yields

$$\begin{aligned}\mathbf{E}_\mathrm{s}(\theta,\phi) \;&=\; \frac{k^2\exp(ikf - i\omega t)}{4\pi\varepsilon_o n^2 f}\left[\mathbf{I} - \mathbf{r}_\infty\mathbf{r}_\infty/f^2\right]\mathbf{p} \\ &\quad\times \exp(-ik[x\sin\theta\,\sin\phi + y\sin\theta\,\cos\phi + z\cos\theta])\end{aligned} \tag{3}$$

where we expressed $(x_\infty, y_\infty, z_\infty)$ in spherical coordinates (f,θ,ϕ). For our purposes $k|\mathbf{r}| < 1$ and hence we expand the last exponential term to first order, i.e. $\exp(x) \approx 1 + x$. This substitution makes a later integration over θ and ϕ possible. The lens collimates the field of the dipole and

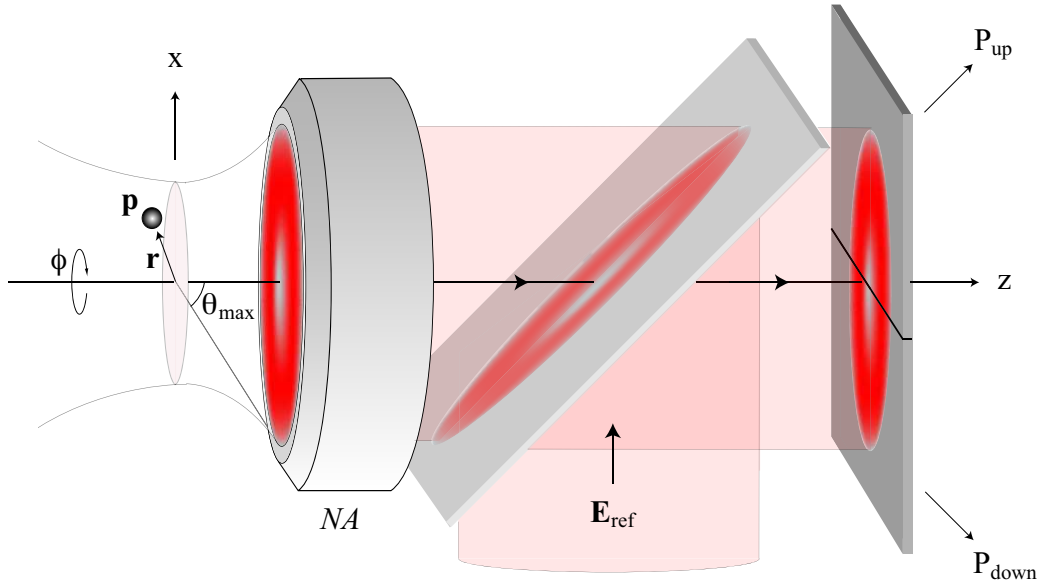

Figure 1: Schematic of detection principle. The field emitted by a dipole $\mathbf{p}$ located at $\mathbf{r}$ is collected with an objective lens (*NA*), then superimposed to a reference field $\mathbf{E}_\mathrm{ref}$, and projected on a split detector rendering two power readings P_up and P_down.

projects it on the plane of the detector. In the detector plane the field can be represented as

$$\begin{aligned}\mathbf{E}_{\rm s}(\theta,\phi) &= \frac{k^2\exp(ik[f+\Delta z]-i\omega t)}{4\pi\varepsilon_o n^2 f}\mathbf{p} \\ &\quad\times(1-ik[x\sin\theta\,\sin\phi+y\sin\theta\,\cos\phi+z\cos\theta])\end{aligned} \tag{4}$$

where Δz is the distance from the lens to the detector plane.

We now superimpose the field to a reference field

$$\mathbf{E}_{\rm r} = iE_{\rm r}\,{\rm e}^{i(k\Delta z-[\omega+\Delta\omega]t-\Delta\phi)}\,\mathbf{n}_{\rm p}\,, \tag{5}$$

where $\mathbf{n}_{\rm p}$ is the unit vector in direction of $\mathbf{p}$, $\Delta\phi$ is a constant phase shift, and $\Delta\omega$ is a frequency shift. As shown in Fig. Figure 1, the split detector employed in our experiment integrates the intensity of the two fields $I(\theta,\phi)\sim|\mathbf{E}_{\rm s}(\theta,\phi)+\mathbf{E}_{\rm r}|^2$ over two halves and yields the two power readings $P_{\rm up}$ and $P_{\rm down}$, from which we calculate the differential signal

$$S = [P_{\rm up}-P_{\rm down}]\,. \tag{6}$$

In terms of the fields $\mathbf{E}_{\rm s}$ and $\mathbf{E}_{\rm r}$ the differential signal becomes

$$S = 2\,{\rm Re}\left\{\int_{\rm up}\mathbf{E}_{\rm r}^*\cdot\mathbf{E}_{\rm s}\,da-\int_{\rm down}\mathbf{E}_{\rm r}^*\cdot\mathbf{E}_{\rm s}\,da\right\}. \tag{7}$$

Only the interference terms survive because the terms $|\mathbf{E}_{\rm s}|^2$ and $|\mathbf{E}_{\rm r}|^2$ are eliminated by subtraction.

Introducing the expressions for $\mathbf{E}_{\rm s}$ and $\mathbf{E}_{\rm r}$ from Eqs. (4) and (5) and carrying out the integrations in Eq. (7) yields

$$S(\mathbf{r}) = \frac{8\pi}{3\varepsilon_o}\frac{NA}{f}\frac{x}{\lambda^3}\,\mathbf{E}_{\rm r}\,{\rm Re}\{\mathbf{n}_{\rm p}\cdot\mathbf{p}\,\exp[i\Delta\omega t+i\Delta\phi]\}, \tag{8}$$

where we made use of the small angle approximation $\sin\theta\approx\theta$. We find that the signal depends

linearly on the dipole's deviation in flow direction (x) measured from the geometric focus $\mathbf{r} = 0$.

The dipole moment $\mathbf{p}$ of the particle is induced by a focused laser field $\mathbf{E}_{\text{exc}}$ and hence

$$\mathbf{p}(\mathbf{r}) = \alpha \mathbf{E}_{\text{exc}}(\mathbf{r}) \,, \tag{9}$$

with α being the polarizability of the particle. For simplicity, we assume that the exciting field is a Gaussian beam of the form

$$\mathbf{E}_{\text{exc}}(x,y,z) = \frac{\mathbf{E}_o \, \mathrm{e}^{ikz}}{(1+2iz/kw_o^2)} \, \mathrm{e}^{-\frac{(x^2+y^2)}{w_o^2} \frac{1}{(1+2iz/kw_o^2)}} \,, \tag{10}$$

where w_o is the beam waist radius. For high NA, Eq. (10) is only a rough approximation and more accurate models for the focal fields are necessary.[1] Fig. Figure 2 shows the calculated signal $S(\mathbf{r})$ for the parameters used in our experiments.[2] The red curve corresponds to the amplitude of $S(\mathbf{r})$ after demodulation with $\exp(i\Delta\omega t)$.

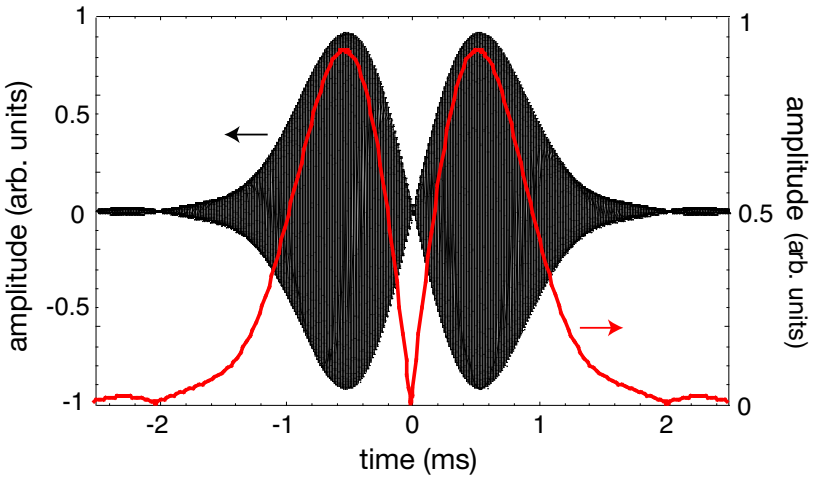

Figure 2: Differential detector signal $S(\mathbf{r})$ for a particle moving along x with speed $v = 1\,\text{mm}$ /sec through the focal plane of a laser beam ($\lambda = 532\,\text{nm}$, $w_o = 0.5\mu m$),obtained via numerical calculations. The reference beam is frequency shifted by 80 kHz. The red curve is the demodulated amplitude.

Experimental Set-Up

The experimental setup is schematically shown in Figure Figure 3. A laser beam from a diode pumped single-mode laser (a) ($\lambda = 532$ *nm*) (Compass 315M-100,Coherent Inc.) is split into two paths using a 90/10 beam-splitter (b). The light transmitted by the beam splitter forms the reference arm of the interferometer, and the reflected beam forms the excitation path. The reflected beam is expanded (i) and sent through an adjustable iris (k). The beam then passes through a 50/50 beam-splitter (l) and is directed into a 10/90 beam-splitter (m). The transmitted beam is

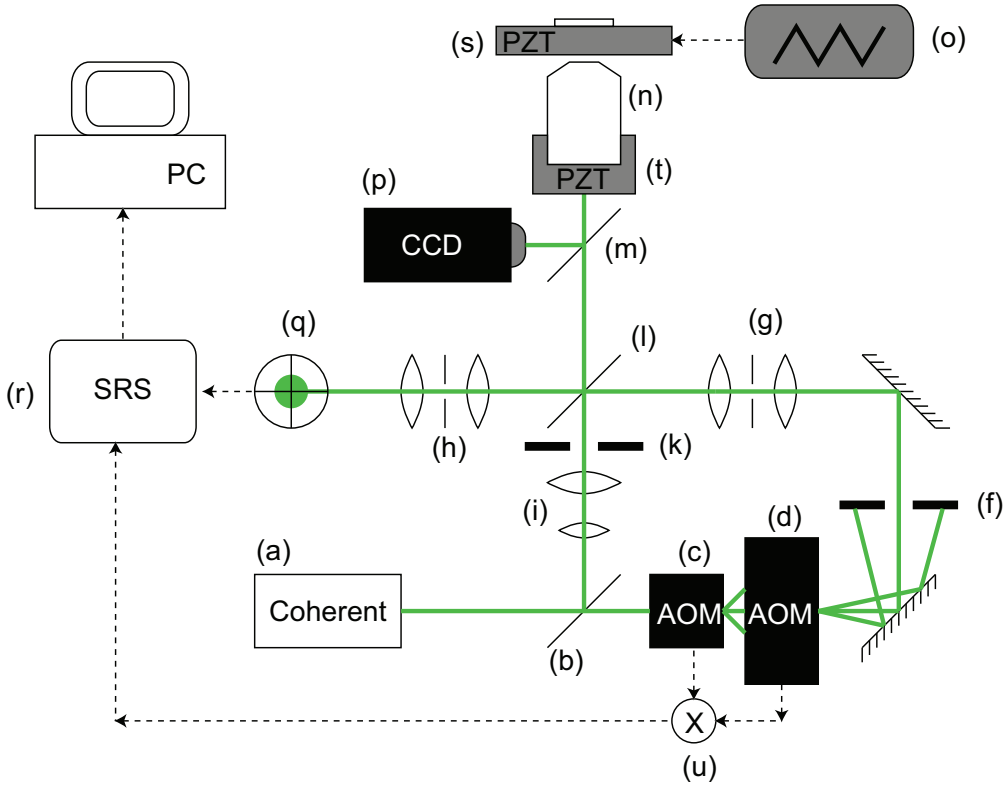

Figure 3: **Experimental configuration,** A ($\lambda = 532nm$) beam from laser (a) is directed into a 10/90 beam-splitter (b). The transmitted beam from (b) is frequency-shifted by the orthogonally oriented AOM-s (c) and (d), and is spatially filtered to form the reference beam for our interferometer.The reflected beam is expanded and directed into the inverted immersion-oil objective (n), which focuses the laser beam into a tight spot. Light scattered from a particle passing through the focal spot is collected by the same objective, and is recombined with the reference beam at the beam-splitter (l) before being directed into the split photodetector (q).The signal from the photodetector is fed into the lock-in amplifier (r), whose X- and Y-outputs are acquired and analyzed using a data-acquisition system and a PC.

then directed into a high-NA oil-immersion objective (n) (Nikon PlanApo,60X,NA 1.4) mounted onto a piezoelectric positioning stage (t) used for translating the objective along the optical axis z. The effective NA of the objective can be controlled by the iris (k). A piezoelectric scanning stage (s)(PI P-733K061) is used to support and translate the nanoparticle sample. The light scattered by a particle crossing the laser focus is collected by the focusing objective. Part of the scattered light is reflected by the beam splitter (m) and directed onto a CCD camera (p). The rest of the scattered light is recombined with the reference beam at the beam splitter (l) and directed toward the split photodetector (q)(Hamamatsu S5990-01) recording the powers P_{up} and P_{down}. The position of the photodetector is adjusted such that the differential signal $S = [P_{\text{up}} - P_{\text{down}}]$ is zeroed in the absence of any particles passing through the laser focus. Frequency-shifting of the reference beam is achieved using two orthogonally oriented acousto-optic modulators [AOM-s (c) and (d)](Isomet 1205C-2).The first-order diffracted beam coming out of the first AOM (c) undergoes a 80.08 MHz frequency shift whereas the negative first-order diffracted beam coming out of the second AOM (d) undergoes a -80 MHz frequency shift. Iris (f) is used to select the desired diffraction order and renders a reference beam that is shifted by 80 kHz with respect to the original laser beam. Spatial filters (g) and (h) are used to obtain uniform phase fronts in the reference and the scattered beams to maximize the heterodyne interferometric oscillations. The signal from the split photodetector is processed by a lock-in amplifier (r)(Stanford Research Systems,SR830), which uses the electronically mixed AOM voltages (u) as the reference waveform. The outputs of the lock-in, as well as the signal generated by the photodetector are digitized using a National Instruments data acquisition card (PCI-6052E) and analyzed in a custom-written Labview software.

Nanofluidic Channels

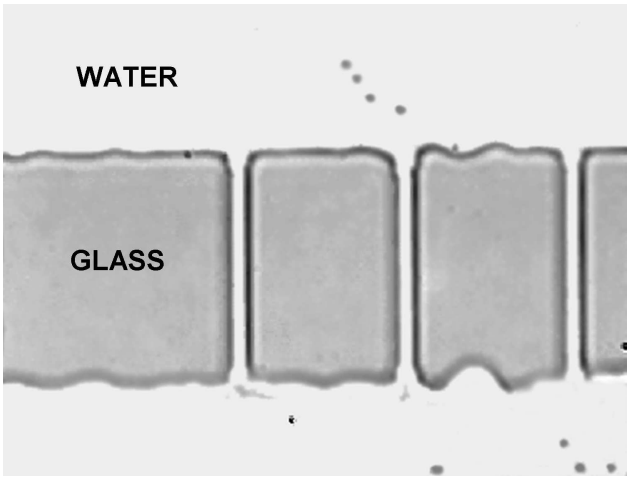

Figure 4: Micrograph of nanofluidic channels fabricated into a borosilicate glass wafer. Nanoparticles are transported from a bottom reservoir through the nanochannels (cross section 500 nm, length 15 μm) to a top reservoir by the electroosmotic effect or are pressure-driven. One of the nanochannels is selected and the laser focus is placed at its center to detect the passage of individual nanoparticles.

Comparison between Heterodyne and Homodyne Detection Schemes

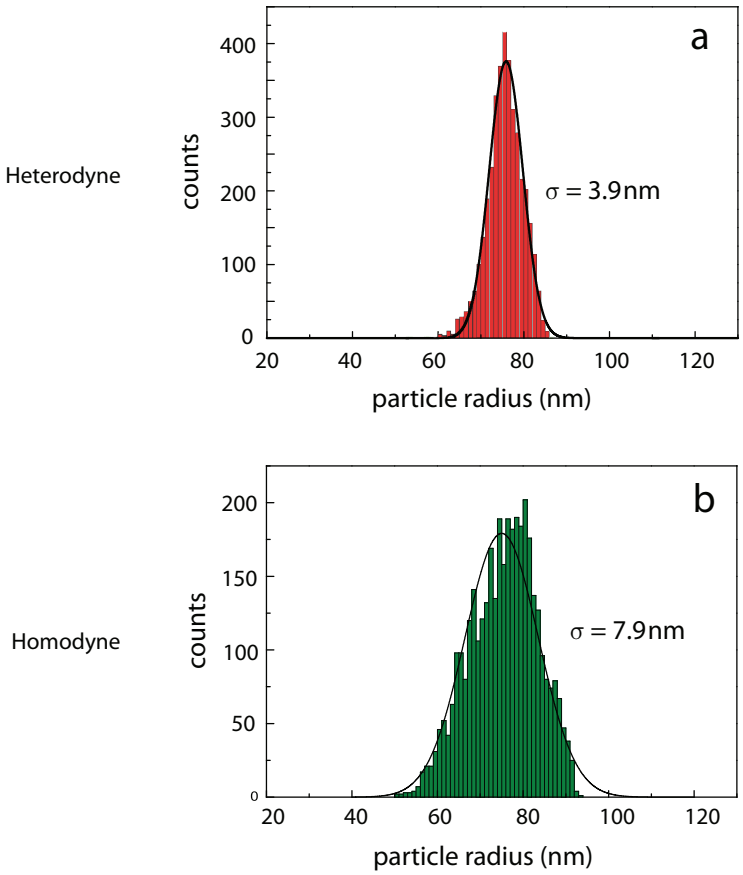

Figure 5: Particle Size Resolution measured for a single 75 nm polystyrene particle electroosmotically trapped in a nanochannel using the (**a**) Heterodyne and (**b**) Homodyne detection schemes. Note the increased width of the distribution in the Homodyne case, which is a result of phase variations due to different particle trajectories. Elimination of phase in the heterodyne scheme clearly decreases the distribution width, hence improving the resolution of particle size-determination.

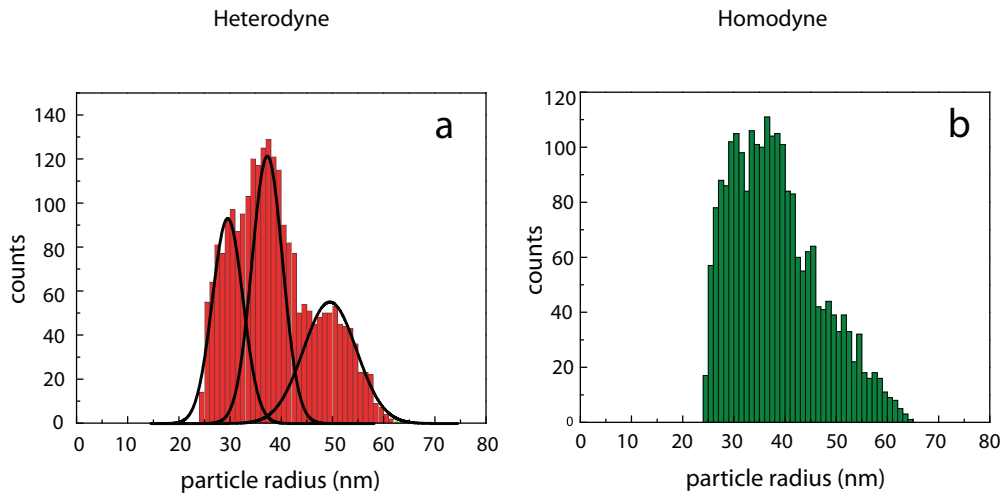

Figure 6: Particle Size Distributions measured for a mixture of 30 nm, 40 nm, and 50 nm gold nanoparticles flowing through a nanochannel using the (**a**) Heterodyne and (**b**) Homodyne detection schemes. Note that one can resolve the particles in the heterodyne case, whereas the distribution is too broad to identify individual particle peaks in the homodyne case.

References

1. Novotny, L.; Hecht, B. *Principles of Nano-Optics*; Cambridge University Press: Cambridge, 2006.

2. Ignatovich, F. V.; Hartschuh, A.; Novotny, L. Detection of Nanoparticles Using Optical Gradient Forces. *J. Mod. Opt.* **2003**, *50*, 1509–1520.